Modulation of Troponin T Molecular Conformation and Flexibility by Metal Ion Binding to the NH_2-Terminal Variable Region†

Jian-Ping Jin*,‡ and Douglas D. Root§

Department of Physiology and Biophysics, Case Western Reserve University School of Medicine, 10900 Euclid Avenue, Cleveland, Ohio 44106-4970, and Department of Biological Sciences, Division of Biochemistry, University of Northern Texas, Denton, Texas 76203-5220

Received November 30, 1999; Revised Manuscript Received June 12, 2000

ABSTRACT: Troponin T (TnT) plays an allosteric signal transduction role in the actin thin-filament-based Ca^{2+}-regulation of striated muscle contraction. Developmentally regulated alternative RNA splicing produces TnT isoforms differing in their NH_2-terminal structure. Physical property variations of the NH_2-terminal hypervariable region of TnT may have a role in tuning the Ca^{2+}-sensitivity and overall cooperativity of the muscle. We have previously demonstrated that metal ion or monoclonal antibody binding to the NH_2-terminal region can modulate the epitopic conformation and troponin I and tropomyosin binding affinity of TnT. To further establish the molecular basis of this conformational and functional modulation, we have characterized the NH_2-terminal variable region-originated secondary conformational effect in TnT using fluorescence spectral analysis. The chicken fast skeletal muscle TnT isoform, TnT8e16, containing a cluster of transition-metal ion binding sites (Tx) in the NH_2-terminal variable region was used in this study. TnT8e16 was titrated for Cu(II) binding-induced changes in fluorescence intensity and anisotropy of the COOH-domain Trp residues (W234, W236, and W285), which demonstrated considerable environmental sensitivity in TnT denaturation studies. Nonlinear Stern−Volmer plots of Trp quenching indicated a metal ion binding-induced conformational change in TnT. Fluorescence anisotropy changes upon metal ion binding indicated a decrease in the mobility of the Trp residues and an increase in the flexibility of fluorescein-labeled Cys263 in the COOH domain. These data support a model that the alternatively spliced NH_2-terminal variable region of TnT modulates conformation and flexibility of other domains of the protein.

Troponin T (TnT)[1] is the tropomyosin (Tm)-binding subunit of the troponin complex and an essential component in the thin-filament regulatory system of striated (cardiac and skeletal) muscle (*1*−*4*). Multiple TnT isoforms are encoded by the cardiac and skeletal muscle TnT genes through developmentally regulated alternative mRNA splicing (*5*−*9*). This seemingly complex regulation is shown by the generation of multiple fast skeletal muscle TnT isoforms, which involves differential splicing of more than six alternative exons (i.e., 4−8, fetal, and additional ones found in birds) corresponding to a highly variable NH_2-terminal region and a pair of mutually exclusive exons (16 and 17) encoding a COOH-terminal segment (*6*, *9*−*12*). Alternative inclusion of an NH_2-terminal acidic segment encoded by one or many exons is responsible for a large to small, acidic to basic TnT isoform switch during both skeletal muscle and heart development (*5*, *13*, *14*). Alternative cardiac TnT isoform expression is also found in human myocardial disorders (*15*, *16*). Therefore, the physiological and pathological significance of the alternatively spliced TnT isoforms needs to be established.

Biochemical studies on TnT structure−function relationships have dissected the protein into two major functional domains. The COOH-terminal fragment T2 (Figure 1) generated by limited chymotryptic digestion interacts with Tm (*17*, *18*), troponin I (TnI), troponin C (TnC), and actin during the Ca^{2+} regulation of contraction (*17*, *19*−*21*). The NH_2-terminal chymotryptic fragment T1 interacts with Tm, involving the head-to-tail overlap of adjacent Tm molecules in the thin-filament assembly (*17*, *18*). While the central region of TnT (the CB2 fragment shown in Figure 1) is required for anchoring of the troponin complex to Tm (*22*), the developmentally regulated NH_2-terminal variable region of TnT (the CB3 fragment) has not been identified with any definitive binding to other thin-filament proteins (*17*, *19*). Deletion of a large portion of the NH_2-terminal variable region from TnT (e.g., the 26 kDa fragment shown in Figure 1) did not have a significant effect on the Ca^{2+} activation of the thin filament (*22*) or the regulation of actoS1 ATPase (*23*). However, studies on intact TnT have demonstrated

† This study was supported in part by grants from the American Heart Association (to J.-P.J.) and National Institute of Health (AR44737 to D.D.R.).

* To whom correspondence should be addressed. Telephone: (216)-368−5525. Fax: (216)368−3952. E-mail: jxj12@po.cwru.edu.

‡ Case Western Reserve University School of Medicine.

§ University of Northern Texas.

[1] Abbreviations: ABTS, 2,2′-azinobis-(3-ethylbenzthiazolinesulfonic acid); BSA, bovine serum albumin; ELISA, enzyme-linked immunosorbant assay; HRP, horseradish peroxidase; mAb, monoclonal antibody; PAGE, polyacrylamide gel electrophoresis; pI, isoelectric point; PIPES, piperazine-*N*,*N*′-bis(2-ethanesulfonic acid); Tm, tropomyosin; TnC, troponin C; TnI, troponin I; TnT, troponin T; Tx, $[H(E/A)EAH]_{4-7}$.

10.1021/bi9927437 CCC: $19.00
Published on Web 08/25/2000

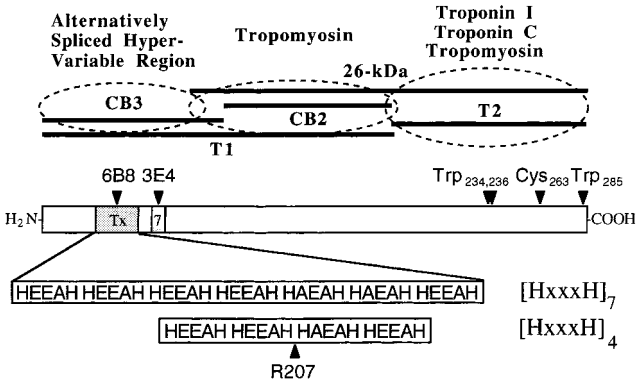

FIGURE 1: Structural domains of TnT and the features of the chicken fast skeletal muscle TnT8e16 isoform. The alternatively spliced NH_2-terminal region and the Tm-, TnI-, and TnC-binding domains of TnT are illustrated with relationships to the T1, T2, CB3, CB2, and 26-kDa fragments of TnT (see the text for detailed description). The three structure−function domains of TnT are outlined by the dashed ovals. A linear illustration of the chicken TnT8e16 polypeptide chain is given with the relevant structural features indicated. Tx indicates the presence of a cluster of seven or four of the H(E/A)EAH metal-binding repeats in the NH_2-terminal variable region. Locations of the epitopes recognized by mAbs 6B8 against the Tx element and 3E4 against the segment encoded by exon 7 and the positions of Trp_{234}, Trp_{236}, Trp_{285}, and Cys_{263} in the COOH-terminal domain are also indicated. The four or seven His pairs flanking three amino acids found in the Tx element of avian breast muscle TnT isoforms are predicted in an α-helical conformation (*28*) and form a cluster of transition-metal ion binding sites (*30*).

differences in the actomyosin ATPase activation by reconstituted thin filaments containing alternatively spliced TnT isoforms differing in the NH_2-terminal structure (*24*). Skinned fiber contractility experiments using muscles expressing TnT isoforms differing in the NH_2-terminal charge showed a difference in their sensitivity to Ca^{2+} activation (*25*). Protein binding assays showed that TnT isoforms with a more acidic NH_2-terminal domain had a higher tolerance to acidosis than did basic isoforms in TnI and Tm binding (*26*).

The lack of crystallography or NMR structure for TnT limits the investigation of the structural and functional role of the NH_2-terminal variable region. To seek alternative approaches, we developed an antibody epitope analysis to monitor the three-dimensional structure of the NH_2-terminal variable domain and the whole molecule of TnT (*27*). Using avian fast skeletal muscle TnT isoforms which contain a transition-metal ion [Zn(II)−, Cu(II)−, Ni(II)−, and Co(II)−] binding segment ($[His-(Glu/Ala)-Glu-Ala-His]_n$, designated as Tx) in the NH_2-terminal variable region (*28*), we have demonstrated that the metal ion binding induces structural changes within the NH_2-terminal Tx segment with secondary effects on the conformation and function of other domains of TnT (*26*, *29*). The binding of Zn(II) or monoclonal antibodies (mAbs) to the NH_2-terminal region of chicken breast muscle TnT induced extensive conformational changes in the protein. This NH_2-terminal domain-originated conformational change has significant effects on TnT's interaction with Tm, TnI, and TnC (*42*), providing a molecular mechanism for the functional significance of TnT isoforms differing in the alternatively spliced NH_2-terminal variable region.

To establish the molecular basis of the TnT conformational and functional modulation, we have further analyzed the NH_2-terminal, variable region-originated, long-range conformational effect in TnT using fluorescence spectral analysis. Chicken breast muscle TnT8e16 containing the metal-binding Tx segment in the NH_2-terminal region was titrated for metal ion-induced changes in fluorescence intensity and anisotropy for three environmentally sensitive COOH-domain Trp residues. The results indicate a metal ion binding-induced conformational change in TnT together with a decrease in the mobility of the Trp residues and an increase in the flexibility of fluorescein-labeled Cys_{263} in the COOH domain. These data support the model that the alternatively spliced NH_2-terminal variable region of TnT modulates the protein conformation and flexibility.

EXPERIMENTAL PROCEDURES

Preparation of Metal-Binding TnT from Chicken Breast Muscle. We have previously demonstrated by cDNA cloning and expression that the adult chicken breast muscle major (pectoralis) contains almost exclusively the fast skeletal muscle TnT8e16 isoform (*26*). TnT8e16 contains seven of the H(E/A)EAH metal-binding sites (*30*) in the NH_2-terminal Tx segment and the mature fast skeletal muscle-specific exon 16 (*31*) in the COOH-terminal variable region (Figure 1). There are three Trp and one Cys residues in the TnT8e16 polypeptide chain (Figure 1). TnT8e16 was purified from fresh breast muscle of adult White Leghorn chicken by a metal-binding affinity chromatography method, taking advantage of the metal-binding Tx element (*26*, *28*). All steps were performed at 4 °C. The muscle tissue was homogenized in 10 mM Tris-HCl, pH 8.0, and the soluble proteins were removed by centrifugation. The myofibril proteins were extracted by 1 M KCl in 10 mM Tris-HCl buffer, pH 8.0, and were subjected to $(NH_4)_2SO_4$ fractionation. The 30−50% saturation fraction was dissolved in 0.1 M sodium phosphate buffer, pH 7.0, containing 1 M NaCl and 6 M urea and loaded on a 15 mL $ZnCl_2$-charged chelating fast flow sepharose (Pharmacia) column as described previously (*28*) for Zn(II)-affinity chromatography. The metal-binding TnT bound to the Zn(II) column was eluted with an imidazole step gradient. The effectively isolated TnT peak identified by SDS−polyacrylamide gel electrophoresis (SDS−PAGE) was dialyzed against 10 mM Tris-HCl, pH 8.0, and concentrated by lyophilization. The sample was then dissolved in 5 mL of 0.1 M sodium phosphate buffer, pH 7.0, containing 1 M NaCl and 6 M urea and loaded on a 120 × 2.5 cm Sephadex G75 (Pharmacia) column for gel filtration chromatography in the same buffer to purify the metal-binding chicken fast skeletal muscle TnT to homogeneity.

Purification of Tx-Negative Low-Molecular-Weight TnT from Chicken Leg Muscle. We have demonstrated previously that the adult chicken leg muscle contains only low-molecular-weight fast TnT isoforms that lack the Tx-metal binding element (*25*, *26*). Following homogenization and washing of fresh muscle in 50 mM KCl to remove soluble proteins, troponin was extracted by 0.75 M $LiCl_2$ at pH 4.5. The supernatant was adjusted to pH 7.5 and then lowered to pH 4.5 to precipitate Tm. Troponin in the supernatant was then fractionated by $(NH_4)_2SO_4$ at 35−65% saturation, and the precipitate was dialyzed against 0.01 N HCl until conductivity was less than 2 mS/cm. The pH of the solution was raised to 4, and the supernatant was clarified by centrifugation to remove TnC. Urea was added to the supernatant to 6 M, and the TnT−TnI mixture was fraction-

ated by CM52 cation-exchange chromatography at pH = 4. The column was developed by a 0−500 mM NaCl gradient. The TnT peak were identified by SDS−PAGE and dialyzed against 0.01% formic acid to remove urea and salt and lyophilized. To further purify the Tx-negative TnT to homogeneity, the lyophilized powders were dissolved in 6 M urea and 20 mM Tris-HCl, pH 8.0, for fractionation by DE52 anion-exchange chromatography. Pure TnT eluted from the column was dialyzed against 0.01% formic acid and lyophilized.

Analytical Cu(II)- and Zn(II)-Affinity Chromatography. Purified chicken TnT8e16 and TnT3e17 (*10*) and rabbit skeletal muscle TnT (*32*) were dissolved alone or as a mixture (2 mg each) in 50 mM sodium phosphate buffer, pH 7.0, containing 3 M urea and 1 M NaCl for a sample volume of 6 mL. The sample was loaded onto a 5 mL chelating fast flow Sepharose Zn(II)- or Cu(II)-affinity column. Following collection of the flowthrough, the column was washed with 5 bed-volumes of the same buffer containing 2 mM imidazole. The bound proteins were eluted by a imidazole step gradient of 2−500 mM (80 mL total) for the Cu(II) column or 2−110 mM (30 mL total) for the Zn(II) column, respectively, in the same buffer. The fractions were analyzed by 14% SDS−PAGE with an acrylamide/bisacrylamide ratio of 37.5:1 to determine the metal-binding property of the TnT isoforms.

Specific Anti-Tx and Anti-TnT Antibodies. Two mAbs, 3E4 and 6B8, raised against chicken breast muscle TnT immunization (*27*) were used in this study. By the use of four cloned chicken TnT isoforms differing in the alternatively spliced NH_2-terminal region *(27*), Western blot have demonstrated that mAb 3E4 recognizes a four amino acid segment (Ala−Pro−Pro−Pro) in the NH_2-terminal variable region encoded by the alternatively spliced exon 7 (Figure 1), whereas mAb 6B8 recognizes the NH_2-terminal Tx element containing four or seven of the H(E/A)EAH metal-binding sites (Figure 1), similar to the specificity of the anti-Tx peptide antibody R207 (*28*). A polyclonal anti-TnT antiserum, RATnT, recognizing all TnT's despite their NH_2-terminal variations (*27*) was used to monitor multiple epitopes on TnT molecule.

ELISA Epitope Analysis. Solid-phase enzyme-linked immunosorbant assay (ELISA) epitope analyses (*27, 29*) were applied to monitor the conformational changes in TnT induced by the binding of metal ions to the Tx segment in the NH_2-terminal variable region. Both primary conformational changes within the Tx element and the secondary conformational changes induced in other domains of TnT were analyzed. Modified from the protocol previously described (*27*), 100 μL/well reaction ELISA was carried out for the epitope analysis. Purified TnT8e16 was dissolved in buffer A (100 mM KCl, 3 mM $MgCl_2$, 10 mM piperazine-*N*,*N*′-bis(2-ethanesulfonic acid) (PIPES), pH 7.0) at 5 μg/mL (0.14 μM) and coated on microtiter plates (Falcon 3915) in the presence of serial dilutions of $ZnCl_2$ or $CuSO_4$. After washing with buffer A plus 0.05% Tween-20 (buffer T) to remove the unbound TnT and blocking the remaining plastic surface with 1% bovine serum albumin (BSA) in buffer T, the immobilized TnT treated with different metal ion conditions was incubated with pretitrated dilutions of the anti-Tx mouse mAb 6B8 or polyclonal rabbit antipeptide antibody R207 in buffer T containing 0.1% BSA. After washes with buffer T to remove the unbound first antibody, the microtiter plates were further incubated with HRP-conjugated anti-mouse immunoglobulin or antirabbit immunoglobulin second antibody, followed by washes and H_2O_2−2,2′-azinobis(3-ethylbenzthiazolinesulfonic acid) (ABTS) substrate reaction. An $A_{405\,nm}$ curve for each assay well was recorded by an automated microplate reader (BioRad Benchmark), and data points from the linear course of the color development were plotted to quantify the conformational changes in the Tx epitope detected by the anti-Tx antibodies.

To examine the secondary conformational changes induced by binding of metal ions to the NH_2-terminal Tx element, chicken TnT8e16 was coated on the microtiter plates in buffer A containing 20 μM $CuSO_4$. After being washed and blocked as above, the plates were incubated with serial dilutions of the mAb 3E4 or the polyclonal RATnT against epitopes outside of the Tx segment. Following washes and second antibody reaction as above, a H_2O_2−ABTS substrate reaction was carried out to detect the binding between the metal ion-treated TnT and the anti-TnT antibodies. The assays were done in triplicates and 20 μM EGTA was used in the TnT-coating solution for the metal free control. An $A_{405\,nm}$ for each assay well was monitored as above, and the data were plotted to analyze the interaction between the antibodies and the specific epitope on TnT molecule. We have previously demonstrated by the ELISA experiments using nonmetal binding chicken fast skeletal muscle TnT isoforms, TnT2e16 and TnT3e17, that the presence of 0.1 mM $ZnCl_2$ had no effect on the coating of TnT to the microtiter plates (*27, 29*).

ELISA Analysis of the Interaction of Metal Ion with Free TnT8e16 in Solution. Modified from the protocols described previously (*26, 27*), microtiter plates were coated with purified rabbit α-Tm (10 μg/mL) in buffer A. After being washed to remove the excess Tm and blocked with buffer T, the plates were incubated with TnT8e16 (0.1 μM) in buffer T containing 0.1% BSA and serial dilutions of $CuSO_4$. The plates were then washed with buffer T to remove unbound TnT before incubation with the polyclonal anti-TnT antibody RATnT. Following washes, HRP-conjugated second antibody was incubated with the plate, followed by washes and H_2O_2−ABTS substrate color reaction. The $A_{405\,nm}$ of triplicate assay wells was monitored and documented as above. Parallel controls with no Tm coating yielded very low backgrounds.

Extinction Coefficient Determination. The extinction coefficient of TnT8e16 at 280 nm was calculated by summing the contributions of absorbances from its component Tyr and Trp residues, the relative ratios of which were verified by second-derivative spectroscopy on an Hewlett-Packard 8453 diode-array spectrometer with 1 nm resolution (*33*). The extinction coefficient at 280 nm in 0.15 M NaCl and 15 mM Tris, pH 7.8, was also directly determined by measuring the absorbance under native buffer conditions followed by dilution of the same sample in urea and remeasurement of the absorbance. The calculated relative extinction coefficients under the two conditions are then used to correct the extinction coefficient determined in urea to the renatured condition.

Fluorescein Labeling of the Chicken TnT8e16. Lyophilized TnT8e16 was dissolved completely in 0.5 M KCl, 6 M urea, 10 mM dithithreitol, and 50 mM Tris-HCl, pH 8.0, at 0.5 mg/mL. Unless indicated otherwise, the solution was dialyzed against 0.15 M NaCl and 15 mM Tris-HCl, pH 7.8, for 12

h at 4 °C, and subsequently ultracentrifuged at 100 000*g* for 1 h in a Beckman TL100 at 4 °C. The TnT8e16 in supernatant was labeled, if needed, with fluorescein-5 maleimide at Cys_{263} at a 5-fold molar excess for 3 h at 22 °C. The progress of the reaction was followed by monitoring the increase in fluorescence of the fluorescein-5 maleimide in a SLM Aminco-Bowman II luminescence spectrometer. To confirm that the fluorescence enhancement was due to thiol modification, a positive control using an equal molar concentration of β-mercaptoethanol in the protein-free dialysate was reacted with the fluorescein-5 maleimide which yielded a rate of fluorescence enhancement similar to that of the TnT8e16. As a negative control, the dialysate alone produced negligible fluorescence enhancement of the fluorescein-5 maleimide. Any unreacted fluorescein-5 maleimide was removed by passing the sample through a G-25 Sephadex gel filtration column on a Pharmacia FPLC.

Tryptophan Fluorescence Emission and Quenching. The Trp fluorescence of urea-denatured and renatured TnT8e16 and the Tx-negative chicken leg TnT control was measured by exciting Trp residues specifically at 300 nm and collecting an emission scan at 4 nm band-pass in a SLM Aminco-Bowman II luminescence spectrometer using rectangular quartz cuvettes. Automated Glans-Thompson polarizers were set to "magic angle" settings for all spectral and quenching analyses to correct for possible polarization-induced artifacts. Emission spectra were corrected in software for wavelength-dependent detection and transmission sensitivities through the polarizers and monochromators by comparison to a NIST standard spectral calibration lamp. Because of the weak Trp fluorescence in the renatured state, a TnT8e16 concentration of 7700 nM was used for optimal readings. For titrations with cupric ion, a 0.1 M stock of cupric sulfate was diluted to final concentrations ranging from 0.1 to 1.6 mM during the fluorescence measurements.

Apparent dissociation constants (K_d) for Cu(II) binding to TnT8-e16 were inferred from the fluorescence quenching at the three peak wavelengths by fitting the data by nonlinear curve-fitting using MacCurvefit (by Kevin Rainer) to the following equation that assumes noninteracting Cu(II) binding sites:

$$F = (F_o - B)[1 - C/(K_d + C)] + B$$

in which F is the fluorescence intensity in arbitrary units, F_o is the fluorescence intensity in the absence of the quencher, C is the concentration of Cu(II), and B is the baseline for fluorescence of Cu(II)-bound TnT8e16. This analysis assumes that the tryptophans' fluorescence is largely protected from quenching by direct interaction with Cu(II) in the renatured TnT8e16. Verification of the validity of this assumption depends on comparison of the results with those determined independently by fluorescence anisotropy.

Collisional quenching by acrylamide was measured for both intrinsic Trp fluorescence and fluorescein-5 maleimide-labeled cysteine fluorescence and compared to the quenching of the free Trp amino acid and fluorescein-5 maleimide. Acrylamide was dilutes from a concentrated stock in water (up to 40%). Fluorescence intensities were corrected for small dilution effects. The data were collected at 22 °C and analyzed by Stern−Volmer Plots.

Fluorescence Anisotropy. Fluorescence anisotropy of tryptophan was measured at a central wavelength in the emission spectrum (348 nm) with excitation at 300 nm using the same conditions as in the quenching experiments above. The automated Glans-Thompson polarizers collected readings in an L configuration and calculated the mathematically corrected anisotropy and standard error for each measurement. For automated background subtraction, a matching quartz cuvette with native buffer plus the equivalent concentration of cupric sulfate was measured prior to each anisotropy reading. The reported anisoptropy (A) is described by the following equation:

$$A = (I_{||} - I_{|})/(I_{||} + 2I_{|})$$

in which $I_{||}$ is the corrected fluorescence intensity of vertically polarized emission following vertically polarized excitation and $I_{|}$ is the corrected fluorescence intensity of horizontally polarized emission following vertically polarized excitation.

Fluorescence anisotropy of fluorescein maleimide attached specifically to Cys_{263} was measured in a similar manner except that the concentration of the TnT8e16 was reduced to 120 nM to avoid inner filter effects and the excitation and emission wavelengths were 490 and 520 nm, respectively.

Dissociation constants (K_d) for Cu(II) binding to TnT8e16 were determined by fitting the anisotropy data with nonlinear curve-fitting using MacCurvefit to the following equations that depend on whether the anisotropy changes are increasing (as with Trp) or decreasing (as with fluorescein) upon Cu(II) binding:

$$A = (A_o - B)[C/(K_d + C)] + B \quad \text{for Trp}$$

and

$$A = (A_o - B)[1 - C/(K_d + C)] + B \quad \text{for fluorescein}$$

in which A is the measured fluorescence anisotropy, A_o is the fluorescence anisotropy in the absence of Cu(II), C is the concentration of Cu(II), and B is the fluorescence anisotropy of Cu(II)-bound TnT8-e16. The equations assume that the change in the fluorescence anisotropy is directly proportional to the amount of Cu(II) bound to noninteracting Cu(II) binding sites on TnT8-e16.

Determination of Sedimentation Coefficient for TnT8e16. Zonal ultracentrifugation was performed on TnT8e16 and standards of known sedimentation coefficients. Identical 5−20% sucrose gradients in 0.15 M NaCl and 10 mM Tris, pH 7.8, were formed by FPLC pumps. Standards at 0.5 mg/mL each in a 0.1 mL volume were overlayed onto one gradient, and TnT8e16 at 0.1 mg/mL in a 0.1 mL volume was overlayed onto a separate 2 mL gradient. Both tubes were then ultracentrifuged at 50 000 rpm for 225 min in the swinging bucket rotor for a Beckman TL100 tabletop ultracentrifuge. Following the run, a needle was inserted into the bottom of each tube, and the solution was drawn through the FPLC UV monitor using a peristaltic pump. The volumes corresponding to the peaks of the major protein bands were recorded and plotted versus the known sedimentation coefficients for the standards (*34*, *35*).

Data Analysis. Since the TnT concentrations (100−140 nM for the ELISA experiments and 7700 nM for the optical experiments as indicated above) are far lower than the Zn-

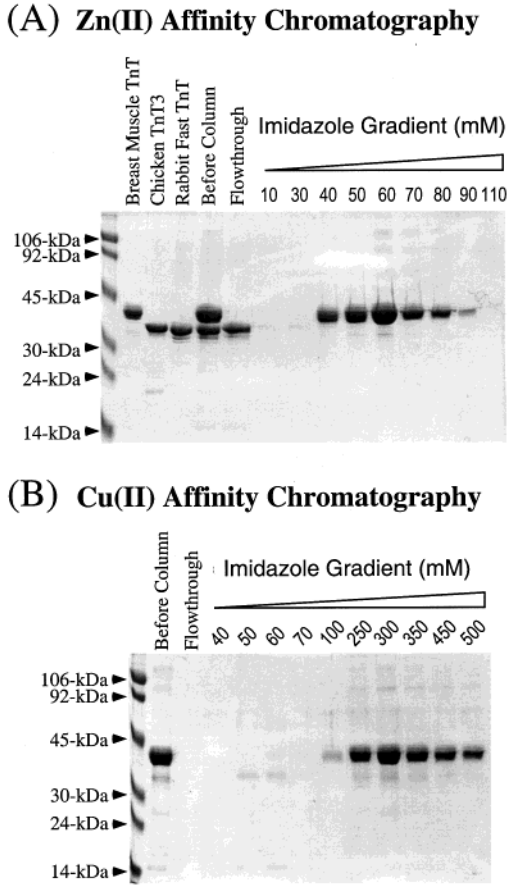

FIGURE 2: Binding of Chicken breast muscle TnT to Zn(II) and Cu(II) in affinity column chromatography. Chicken breast muscle TnT8e16 was analyzed for its Zn(II)- and Cu(II)-binding properties. Purified chicken breast muscle TnT8e16, alone or mixed with TnT3e17 and rabbit skeletal muscle TnT, was loaded onto Cu(II)- or Zn(II)-affinity columns, respectively. The flowthrough and imidazole gradient eluting fractions were analyzed by SDS−PAGE. (A) Zn(II)-affinity chromatography demonstrating that the Tx-negative rabbit skeletal muscle TnT and chicken TnT3e17 did not bind to the column whereas the Tx-positive chicken TnT8e16 specifically bound to the column and was eluted as a peak by competition with the imidazole gradient. (B) Cu(II)-affinity chromatography also demonstrating a specific binding of the chicken TnT8e16. However, the TnT peak was eluted at an imidazole concentration much higher than that shown in the Zn(II) column profile, indicating a significantly higher binding affinity between Cu(II) and the Tx element.

(II) and Cu(II) concentrations used (K_d's), we assumed that free Cu(II) = total Cu(II) and used the total added metal concentrations for plotting the data. The epitope analysis results were plotted as percentage of the maximum binding of the antibodies or as the $A_{405\,nm}$ values without fitting. The metal ion concentrations and mAb dilutions required for 50% maximum binding to the immobilized or free TnT were determined graphically from the titration curves. The collisional quenching of Trp fluorescence by acrylamide and the fluorescence anisotropy of fluorescein were plotted using MacCurvefit software.

RESULTS

Specific Binding of Chicken TnT8e16 to Zn(II) and Cu(II) Affinity Columns. Results of the analytical Zn(II)-affinity chromatography (Figure 2A) showed that the Tx-negative rabbit fast skeletal muscle TnT and chicken fast skeletal muscle TnT3e17 had no binding to the metal-affinity column and were present in the flowthrough fraction. In contrast, the high-molecular-weight Tx-positive chicken breast muscle TnT8e16 (Figure 1) bound to the Zn(II) column and eluted as a single peak around 50−60 mM imidazole. Under identical conditions, chicken TnT8e16 showed a significantly higher binding affinity to the Cu(II) column as the bound TnT was eluted as a peak around 300 mM imidazole (Figure 2B). These results demonstrate that Cu(II) has a significantly higher affinity than that of Zn(II) to the Tx segment in the NH_2-terminal variable region of chicken TnT8e16 and, therefore, can be used as a more effective inducer for the studies of the metal ion−NH_2-terminus binding-induced conformational modulation of TnT.

Zn(II) and Cu(II)-Induced Structural Reconfiguration within the Tx Segment of TnT8e16. Using the anti-Tx peptide antibody R207, we have previously shown that binding of Zn(II) to the Tx element induced local conformational changes within the Tx region (*29*). This Zn(II)-induced allosteric change has been further demonstrated by the metal ion-induced drop of affinity to mAb 6B8 which was raised against native Tx-containing TnT immunogen (*27*). The results in Figure 3A show that both 6B8 and R207 antibodies had decreased affinity to the Tx-containing chicken breast muscle TnT depending on the concentration of $ZnCl_2$ or $CuSO_4$. The changes in specific antibody affinity reflect the metal ion-induced conformational changes in the Tx epitopes. The data further demonstrate the different binding affinities of Zn(II) and Cu(II) to the Tx segment in the NH_2-terminal domain of TnT. The significantly higher affinity of Cu(II) to TnT8e16 measured as the conformational change of the Tx epitopes (Table 1A) agrees with the metal-affinity chromatography results (Figure 2).

Affinity of Free TnT8e16 to Cu(II) in Solution. ELISA experiments with Tm coated on the microtiter plate further analyzed the metal ion-binding affinity of free Tx-positive TnT in solution (Figure 3B). The polyclonal antibody RATnT against multiple epitopes on TnT demonstrated decreased bindings corresponding to the increasing concentration of Cu(II) in the TnT8e16 solution. Together with the metal ion-binding-induced epitope conformational changes in TnT and decrease in affinity to the antibody as shown in Figure 3A, a decrease in TnT's binding affinity to Tm induced by the metal−Tx binding in solution determines the titration curve in the ELISA experiments. Although the result was a combined effect of the two mechanisms (a solid-phase binding was involved and, therefore, it was not a true solution measurement), the titration curve reflects the affinity of TnT8e16 to Cu(II) in solution, an affinity that is significantly lower than that of the immobilized TnT8e16 (Figure 3A). Similar experiments using the anti-Tx mAb 6B8 and the anti-exon 7 segment mAb 3E4 (Figure 1) showed similar results (Table 1), confirming the lower binding affinity of metal ions to the Tx element in free TnT than that in immobilized TnT. The mechanism of this significant difference between the affinity of free and immobilized Tx-TnT for the metal ions remains to be investigated.

The experiments shown in Figure 3B also demonstrate that the effects of metal ion binding to the NH_2-terminal domain of TnT are compatible with the TnT−Tm interaction that requires a two-site binding involving both NH_2- and COOH-terminal domains of TnT in an elongated conformation (*18*).

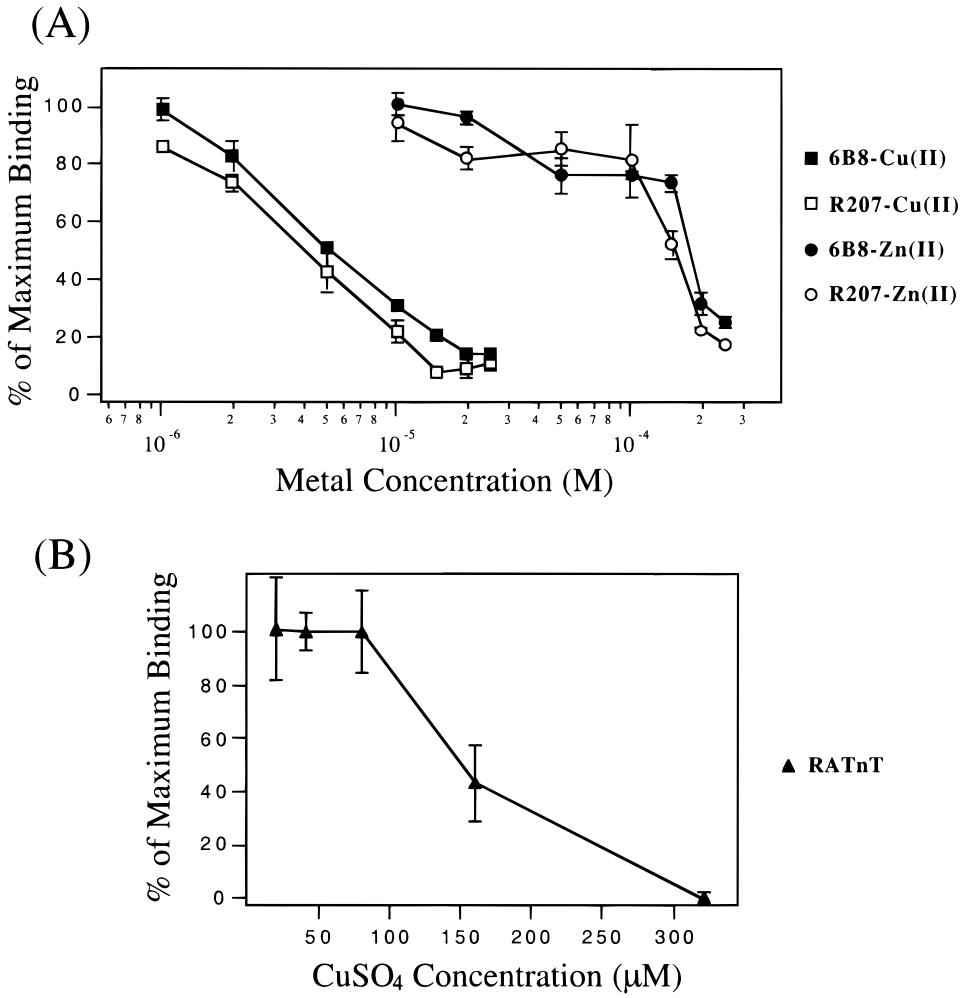

FIGURE 3: Zn(II) and Cu(II) binding to the Tx element in chicken breast muscle TnT reducing the affinity of anti-Tx antibodies. (A) ELISA antibody binding experiments performed on chicken TnT8e16 coated on microtiter plates in the presence of serial dilutions of $ZnCl_2$ or $CuSO_4$. TnT8e16 treated with 20 μM EGTA was used as a control for the maximum antibody binding without the metal ion effect. The results show significant decreases of the binding affinity of mAb 6B8 and anti-Tx peptide antibody R207 depending on the Zn(II) or Cu(II) concentration, indicating that Cu(II) or Zn(II) binding changed the local three-dimensional structure of the Tx segment. The lower [$CuSO_4$] than [$ZnCl_2$] required for this modulation is consistent with the significantly higher affinity of Cu(II) than that of Zn(II) to the Tx element. (B) ELISA experiments carried out with Tm coated on the microtiter plate for evaluation of the metal ion-binding affinity of free Tx-positive TnT in solution. TnT8e16 at 140 nM was mixed with serial dilutions of $CuSO_4$ and incubated with the immobilized Tm. After the unbound TnT and $CuSO_4$ were washed away, a pretitrated dilution of the anti-TnT polyclonal antibody RATnT was added to the plate to detect the effect of Cu(II)−Tx binding in solution on TnT's affinity for Tm via HRP-labeled second antibody and substrate reaction. The titration curve demonstrate a significantly lower binding affinity of the free TnT8e16 to Cu(II) than that of TnT8e16 immobilized on microtiter plates.

Therefore, the data support that the metal ion−Tx binding-induced conformational change in other domains of TnT is a long-range secondary modulation effect (see below) other than a "fold-back" direct contact between Tx and other sites due to a structural flexibility in solution.

The steep metal ion titration curves in Figure 3 showed an apparently cooperative binding of metal ions to Tx in the ELISA experiments. This cooperativity associated with the metal ion binding to Tx involved TnT immobilized to ELISA plate or Tm may be produced by three potential mechanisms: (i) the immobilization may confer a conformation of the cluster of seven HisXaaXaaXaaHis pairs in the Tx segment, which supports an cooperative binding to multiple metal ions; (ii) the cooperativity detected by the affinity change of the anti-Tx antibodies may also partially be contributed by the pliable fitting between the antibody paratope and the Tx epitope structures. In this case, a minimal number of metal ions bound to the Tx cluster may be required to result in a detectable decrease in the antibody affinity; (iii) the repeated washes during the ELISA procedure more effectively remove weaker binding versus strong binding, making the titration curves steeper. As a consequence, the whole change is detected in a narrowed range of metal ion concentration.

Metal−Tx Binding-Induced Secondary Conformational Changes in TnT Detected by Antibody Epitope Analysis. Figure 4A demonstrates a conformational change in the exon 7-encoded epitope induced by the binding of Cu(II) to the Tx element. The results of ELISA epitope analysis showed that $CuSO_4$-treated chicken breast muscle TnT8e16 had significantly decreased reactivity to mAb 3E4 as compared with that in the presence of 20 μM EGTA. Therefore, conformation of the epitope recognized by mAb 3E4 (that is specified by an Ala−Pro−Pro−Pro segment downstream of the Tx sequence intercalated by 5 amino acids (*10*; Figure 1)) was significantly altered as a secondary effect of the

Table 1. Effects of Metal Ion Binding on TnT8e16's Reactivity to Specific Antibodies and Tm

(A) concentrations of metal ions required for 50% inhibition of maximum binding of the anti-Tx antibodies[a]

	antipeptide R207	mAb 6B8
Zn(II)	151.4 μM	177.8 μM
Cu(II)	4.0 μM	5.1 μM

(B) concentrations of metal ions required for 50% inhibition of maximum binding of free TnT8e16 to immobilized Tm and detected by the anti-Tx and anti-TnT antibodies[b]

	6B8	3E4	RATnT
Cu(II)	132 μM	126 μM	150 μM

[a] The metal ion concentrations for 50% inhibition of the maximum antibody binding to the TnT8e16 immobilized onto microtiter plates were determined from data presented in Figure 3A. A significantly higher binding affinity of Cu(II) than Zn(II) to the Tx element in the NH_2-terminal region of TnT is shown. TnT8e16 coated onto microtiter plates in buffer A containing 20 μM EGTA was used to obtain the maximum binding. [b] The concentrations of Cu(II) required for 50% inhibition of maximum binding of free TnT8e16 to Tm coated on microtiter plates as detected by the anti-Tx mAb 6B8, anti-NH_2-terminal mAb 3E4, and polyclonal anti-TnT antibody RATnT were deduced from data represented by Figure 3B.

original conformational changes in the Tx segment. This result indicates that Cu(II) binding not only reconfigured the Tx structure but also induces secondary conformational changes in other regions of the TnT molecule. The results in Figure 4B further demonstrate that the binding of Cu(II) to the NH_2-terminal variable region of chicken TnT8e16 significantly changed the binding avidity of the RATnT polyclonal antibody that recognizes multiple epitopes on TnT. The dramatically diminished reactivity of RATnT indicates that the structure of the TnT molecule was extensively altered as a consequence of the primary conformational change within the Tx region upon the binding of Cu(II).

Quenching of Intrinsic TnT8e16 Trp Fluorescence by Cu-(II). The environmental sensitivities of the absorbance and fluorescence properties of tryptophans in TnT8e16 are demonstrated by their changes upon protein denaturation by urea. On the basis of its Trp and Tyr content, the extinction coefficient at 280 nm of the urea denatured TnT8e16 was calculated to be 25 000 M^{-1} cm^{-1}. This value agreed well with direct empirical measurements of the extinction coefficient at 280 nm of the urea denatured TnT8e16 which yielded a value of 26 000 M^{-1} cm^{-1} based on a calculated molecular mass of 33 802 Da from the cDNA sequence (*26*). In contrast, the extinction coefficient under the renatured condition was 12 000 M^{-1} cm^{-1} at 280 nm, indicating that the three Trp residues in the COOH-terminal domain of TnT8e16 (Trp_{234}, Trp_{236}, and Trp_{285}; Figure 1) have considerable environmental sensitivity. Furthermore, the intensity of Trp fluorescence increased more than four times upon denaturation by urea. Therefore, the fluorescence of these residues is responsive to TnT conformational changes in the COOH-terminal domain (Figure 1).

When fluorescence emission spectra were recorded with excitation at 300 nm in the presence of different concentrations of cupric sulfate, the Trp fluorescence of the renatured TnT8e16 exhibited three peaks at 366, 348, and 327 nm, which may correspond to the three different tryptophans in the primary sequence (Trp_{234}, Trp_{236}, and Trp_{285}). A reduced

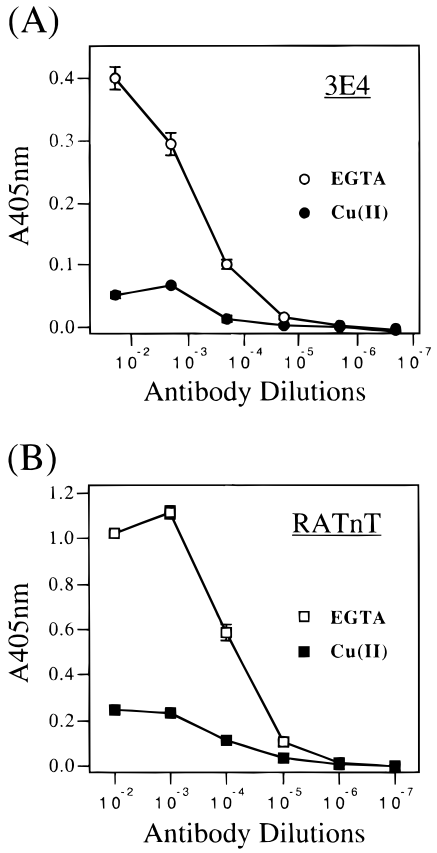

FIGURE 4: Cu(II)−Tx interaction-induced conformational changes detected by epitope analysis using antibodies against sites outside of the Tx region. (A) In the presence of 20 μM $CuSO_4$ or 20 μM EGTA, Cu(II) binding to the NH_2-terminal Tx segment inducing a secondary conformational effect on the downstream exon 7-encoded epitope (Figure 1), shown by the significant decrease of mAb 3E4 binding affinity. (B) Cu(II) binding to the NH_2-terminal Tx segment with extensive conformational effects on the whole TnT molecule as demonstrated by the significant decrease in binding avidity of the polyclonal RATnT antiserum, which recognizes multiple epitopes in both NH_2- and COOH-terminal domains of TnT.

degree of fluorescence quenching at 327 nm was present relative to the other peaks. The 327 nm peak is no longer resolved upon denaturation by urea, although the peaks at 348 and 366 nm are still apparent, and their persistence may reflect interactions with neighboring amino acids in the primary sequence. It is possible that the fluorescence emission peaks at 348 and 366 nm of the renatured TnT8e16 correspond to tryptophans in more similar environments, and Trp_{234} and Trp_{236} are likely to be in similar environments due to their close proximity in the primary structure. The results in Figure 5A show that Cu(II) quenched the peaks at 348 and 366 nm more rapidly than it did the peak at 327 nm, corroborating the suggestion of a different environment for the Trp responsible for this fluorescence. The quenching of intrinsic TnT8e16 Trp fluorescence by Cu(II) indicates that the binding of metal ions to the Tx element in the NH_2-terminal variable induces significant conformational changes in the COOH-terminal domain where the three Trp residues are present (Figure 1).

Dissociation constants of Cu(II) binding to the Tx element in the NH_2-terminal region of TnT8e16 containing seven of the H(E/A)EAH metal-affinity sites (Figure 1) under the experimental conditions were deduced from the intrinsic Trp fluorescence quenching experiments (Figure 5B). The af-

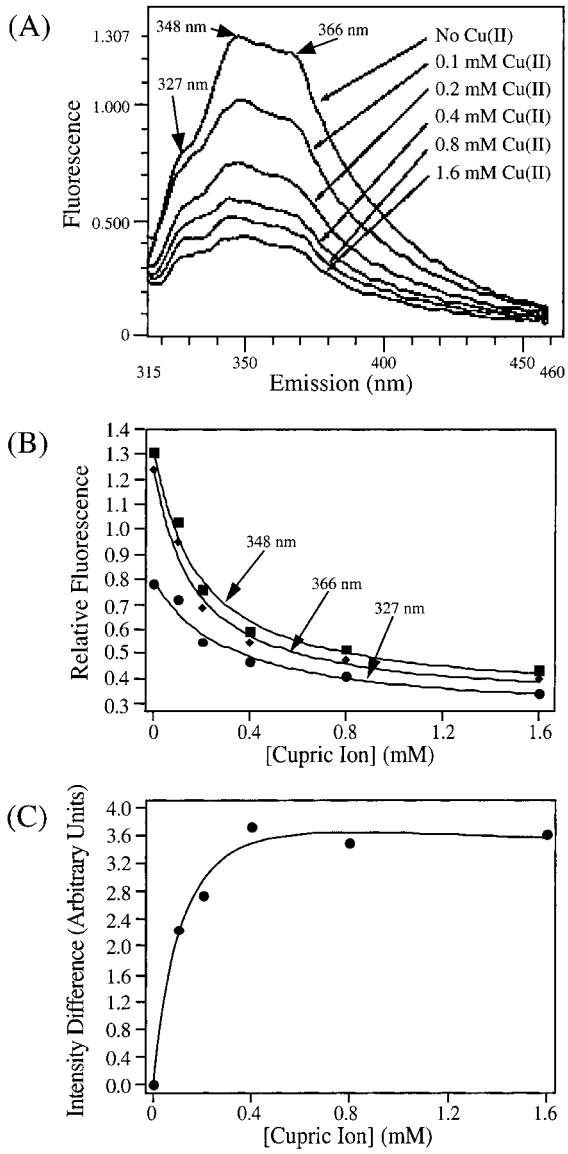

FIGURE 5: Intrinsic TnT8e16 Trp fluorescence and quenching by Cu(II). (A) Fluorescence emission spectra recorded with excitation at 300 nm of 7700 nM TnT8e16 in the presence of different concentrations of cupric sulfate. Note the three peaks in the Trp fluorescence emission and the reduced degree of fluorescence quenching at 327 nm relative to the other peaks. (B) Estimation of dissociation constants for Cu(II) binding to TnT8e16 based on concentration-dependent fluorescence quenching of Trp fluorescence by Cu(II): 327 nm, $K_d = 0.30 \pm 0.10$ mM; 348 nm, $K_d = 0.18 \pm 0.05$ mM; 366 nm, $K_d = 0.17 \pm 0.04$ mM. See Experimental Procedures for the nonlinear curve-fitting procedures. The correlation coefficient, r^2, was greater than 0.96 in all cases. (C) Extraction of the fluorescence from the Trp with a peak at 327 nm by difference spectroscopy. The analysis is done as follows. Definitions: I_2(Cu) is the sum of intensities as a function of Cu(II) concentration of the tryptophans with peaks at 368 and 348 nm. I_1(Cu) is the intensity as a function of Cu(II) concentration of the Trp with a peak at 327 nm. I(Cu) is the sum of intensities as a function of Cu(II) concentration of all three tryptophans. R is the ratio of $I_2(0)/I_2$(Cu) which is constant at any wavelength. ($I_2(0)$ is I_2(Cu) at [Cu(II)] = 0). Given: I(Cu) = I_2(Cu) + I_1(Cu) and $I(0) = I_2(0) + I_1(0)$. Then: RI(Cu) − $I(0) = RI_2$(Cu) + RI_1(Cu) − $I_2(0) - I_1(0)$ and RI(Cu) − $I(0) = RI_1$(Cu) − $I_1(0)$. The quantity RI(Cu) − $I(0)$ is measured as a function of wavelength and Cu(II) concentration. The equation in the Experimental Procedures can be substituted into this final equation, since I_1(Cu) is the same as F defined in Experimental Procedures. When this is done, a nonlinear least-squares fit of the data yields a K_d of 0.2 ± 0.1 mM for the Trp with a peak at 327 nm.

finities of Cu(II)−Tx binding determined by this direct measurement of the induced TnT conformational change (Table 2) are significantly lower than that reflected by the Cu(II) titration of the anti-Tx antibody affinity against TnT8e16 immobilized on the microtiter plates (Table 1A). However, the K_d values determined by the fluorescence measurements are similar to that evaluated by the ELISA experiment on free TnT8e16 in solution (Figure 3B and Table 1B). Therefore, the effects of immobilization of TnT onto the microtiter plates may result in altered allosteric characteristics in contrast to the TnT in solution, which allows a higher accessibility of the Tx cluster by the metal ions.

Extraction of the fluorescence from the Trp with a peak at 327 nm was done by difference spectroscopy (Figure 5C). A nonlinear least-squares fit of the data yielded a K_d of 0.2 ± 0.1 mM for this Trp. The dynamic quenching equations do not yield a good fit to the data, confirming that the primary source of quenching is due to binding by Cu(II) to TnT. This analysis supports the contention that all three tryptophans are affected by Cu(II) binding to the NH_2-terminal region. It also suggests that the Trp with a peak fluorescence at 327 nm is the lone COOH-terminally located Trp_{285}.

Cu(II)-Induced Conformational Changes Cause Quenching of Trp Fluorescence of TnT8e16. Figure 6A demonstrates the lower accessibility to collisional quenching by acrylamide of the intrinsic TnT8e16 Trp fluorescence relative to free Trp. The results indicate that the three COOH-terminal Trp residues in TnT are protected by tertiary structures and may be used as indicators for the conformational changes in the TnT molecule. In contrast, little difference was observed in the quenching of fluorescein-5 maleimide-labeled TnT8e16 and free fluorescein-5 maleimide, indicating a high degree of accessibility of the COOH-terminal Cys_{263} to the solvent (Table 2), so direct collisional quenching dominated the signal changes observed at this site. The linear Stern−Volmer plots are consistent with a dynamic quenching mechanism for acrylamide and the quenching of free Trp by Cu(II). Figure 6B shows the quenching of intrinsic TnT8e16 Trp fluorescence by Cu(II). The data again indicate a protection of the tryptophans by the protein structure. Different from the feature of the Tx-negative TnT, the nonlinear Stern−Volmer plot further demonstrates that the quenching is not due to a dynamic mechanism but reflects quenching due to a conformational change in TnT8e16 induced by Cu(II) binding to the NH_2-terminal Tx site. In addition, the quenching by Cu(II) of the three peaks of the Tx-negative TnT was very similar, in contrast to the Tx-positive emission spectra in which the 327 nm peak was quenched more slowly than the others. Also, the relative intensities of the three peaks are slightly different in the two TnT's.

Fluorescence Anisotropy Changes of TnT8e16 in Response to Cu(II) Binding. Figure 7A shows the fluorescence anisotropies of intrinsic Trp fluorescence of TnT8e16 measured together with the Tx-negative TnT by excitation and emission at 300 and 348 nm, respectively. Distinct from the Tx-negative chicken leg TnT, the Cu(II)-induced changes in TnT8e16 are consistent with Cu(II) binding with a dissociation constant of 0.25 ± 0.02 mM, which is similar to the values obtained from direct fluorescence quenching in Figure 5B. There was a decrease in the overall rotational flexibility of the tryptophans (Trp_{234}, Trp_{236}, and Trp_{285}) in the COOH-terminal domain of TnT upon Cu(II) binding to

Table 2. Summary of Spectral Observations on the Chicken Metal-Binding TnT

residue(s)	method	K_d for Cu(II)	accessibility	flexibility
Trp (366 nm)	Cu (II) quenching	0.17 ± 0.04 mM	protected	N/A[a]
Trp (348 nm)	Cu (II) quenching	0.18 ± 0.05 mM	protected	N/A
Trp (327 nm)	Cu (II) quenching	0.3 ± 0.1 mM	very protected	N/A
Trp (348 nm)	anisotropy	0.25 ± 0.02 mM	protected	Cu(II) decreases flexibility
Cys (fluorescein)	anisotropy	0.21 ± 0.02 mM	highly accessible	Cu(II) increases flexibility
Cys	chemical reactivity	N/A	highly accessible	N/A
Cys (fluorescein)	acrylamide quenching	N/A	highly accessible	N/A
Trp (348 nm)	acrylamide quenching	N/A	protected	N/A
Trp	denatured fluorescence	N/A	4× increase	N/A
Trp	denatured absorbance	N/A	2× increase	N/A

[a] N/A: not applicable.

the NH_2-terminal Tx element (Figure 1). In contrast, Figure 7B shows that the fluorescence anisotropies of fluorescein-5 maleimide-labeled Cys_{263} in TnT8e16 upon the addition of Cu(II) indicated an increase in rotational flexibility of this region of the COOH-terminal domain of TnT. Similar to the results with Trp fluorescence, the changes in fluorescein-5 maleimide fluorescence are consistent with a dissociation constant of 0.21 ± 0.02 mM for Cu(II) binding. Zn(II) induced qualitatively similar changes in that it increased the Trp fluorescence anisotropy of TnT8e16 and decreased the fluorescence anisotropies of fluorescein-5 maleimide-labeled Cys_{263}; however, much higher (5−50 mM) concentrations of Zn(II) were necessary to induce a response, and the background from these high Zn(II) concentrations limited the quantitative analysis of the data (not shown). These results provide evidence that the binding of metal ions to the NH_2-terminal region of TnT induces not only long-range conformational changes but also changes in the flexibility of the protein structure.

The Trp quenching and anisotropy properties of Tx-negative TnT were significantly different from that of the Tx-positive TnT8e16. The nearly linear metal ion titration curves may represent the effects of direct quenching by Cu(II) of Trp fluorescence in the Tx-negative TnT which affects both the fluorescence intensities and the fluorescence lifetimes and thereby also the fluorescence anisotropies of the tryptophans (Figures 6B and 7A). In contrast, the fluorescence changes of TnT8e16 with Cu(II) cannot be explained by simple collisional quenching.

Troponin T Remains a Monomeric Elongated Conformation under the Experimental Conditions. The sedimentation coefficient of 2.3 ± 0.3 $s_{20,w}$ for TnT8e16, determined as shown in Figure 8, indicates that the TnT8e16 is primarily monomeric given the known monomeric molecular weight of 34 kDa. By contrast, the dimeric Tm has a sedimentation coefficient of 2.6; so if TnT8e16 were dimeric, it would have to be at least as elongated as Tm, which is not consistent with the postulated structural models of TnT. On the other hand, the sedimentation coefficient is low enough that it is clear that TnT8e16 is in an elongated conformation in solution, precluding the possibility of a fold-back direct contact between the NH_2-terminal Tx and the COOH-terminal domain. The theoretical minimum sedimentation coefficient for a perfectly spherical TnT8e16 is 4 $s_{20,w}$ which is much larger than that measured. This difference can be used to estimate a maximum axial ratio of approximately 10 which is consistent with a very elongated structure that supports current structural models of TnT in which the NH_2- and COOH-terminal domains are widely separated in the three-dimensional structure.

DISCUSSION

The reported results demonstrate a correlation between metal ion-induced conformational changes in the NH_2-terminal domain of TnT8e16 and conformational changes in its COOH-terminal domain. The evidence for metal ion-induced changes in the conformation of the NH_2-terminal domain includes the presence of the Tx sequence that has differential affinity for metal ions, as shown by affinity chromatography and the changes in epitope structures in the NH_2-terminal domain upon binding metal ions. Conformational changes in the COOH-terminal domain are demonstrated by independent changes in fluorescence intensity and anisotropy of both Trp and fluorescein-5 maleimide-labeled Cys residues. These data suggest that structural changes in the NH_2-terminal variable region of TnT may affect the function of the entire molecule in the regulation of muscle contraction.

Metal Ion Binding-Induced Conformational Changes within the Tx Segment and Secondary Effects on the Conformation of Whole TnT. As we have shown previously, the binding of Zn(II) to the Tx segment alters the three-dimensional structure of the Tx segment residing in the TnT protein (Figure 3). This original structural reconfiguration further affects the conformation of epitopes outside of the Tx region as demonstrated by the change in the binding affinity of mAb 3E4 (Figure 4A) that recognizes a downstream epitope (Figure 1) and the polyclonal antibody RATnT that recognizes multiple epitopes (Figure 4B). The results demonstrated that the conformational reconfiguration within the Tx region is transduced to other epitopic structures of TnT. The similar results of the Zn(II)- and Cu(II)-binding experiments indicate that this NH_2-terminus originated conformational modulation of TnT is independent of the use of particular transition-metal ions. Therefore, it may exemplify a universl mechanism in which reconfigurations of the NH_2-terminal variable region structure modulates the overall conformation and function of TnT.

Metal−Tx Binding-Induced Conformational Modulation of TnT Revealed by the Spectral Analysis Agrees with That Detected by the Antibody Epitope Analysis. We previously showed by antibody epitope analysis that Zn(II) binding to the NH_2-terminal domain of TnT reconfigures the global conformation of TnT (*27*), and this is also true for the Cu(II)−Tx binding (Figures 3 and 4). The present study further demonstrated this intramolecular conformational modulation

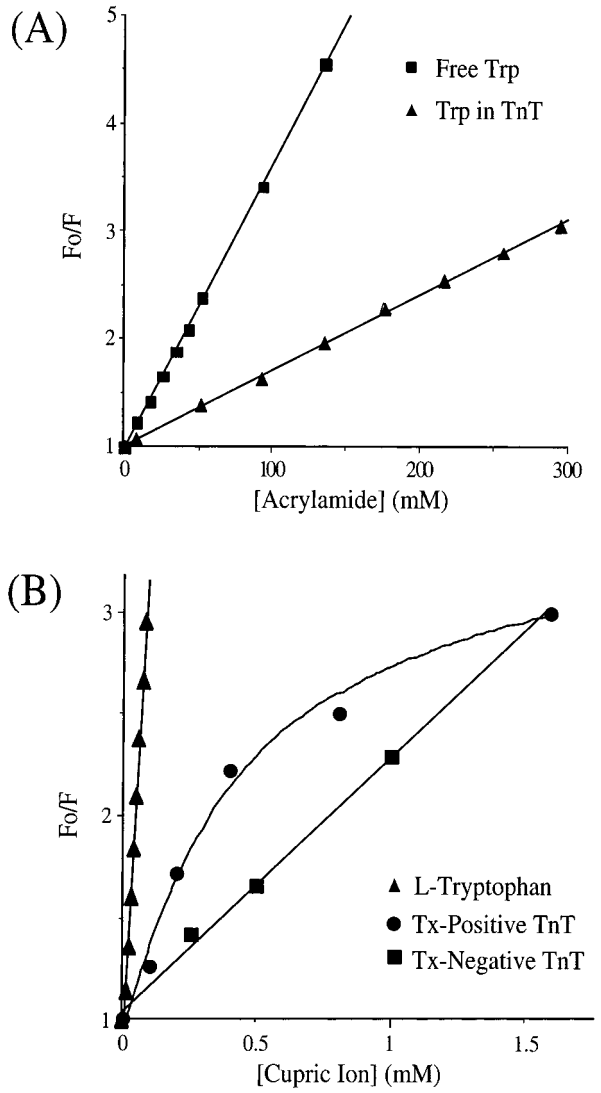

FIGURE 6: Stern−Volmer plots of TnT8e16 Trp fluorescence quenching by (A) acrylamide and (B) Cu(II). The fluorescence of TnT8e16 at 7700 nM was monitored at 348 nm. The lower accessibility to collisional quenching by acrylamide of the intrinsic TnT8e16 Trp fluorescence relative to free Trp is illustrated. Linear Stern−Volmer plots are consistent with a dynamic quenching mechanism for acrylamide and the quenching of free Trp by Cu(II). In contrast to the linear Stern−Volmer plots produced by the quenching of intrinsic Trp fluorescence of Tx-negative TnT by Cu(II), indicating a protection of the tryptophans by the protein structure and reflecting some nonspecific weak binding of Cu(II) to the protein, the Cu(II) quenching of intrinsic Tx-positive TnT8e16 Trp fluorescence produced a nonlinear Stern−Volmer plot which is consistent with quenching due to a conformational change in TnT8e16 induced by Cu(II) binding to the Tx segment.

by direct analysis of Trp fluorescence. The results clearly demonstrated Cu(II) binding to the NH_2-terminal Tx element-induced conformational changes in the Trp residues in the distant COOH-terminal domain of TnT. These data provide evidence to verify the reliability of the ELISA antibody epitope analysis as an effective approach for monitoring protein conformation and structural dynamics (*36*). The application of site-specific mAb's is able to identify conformational changes in certain regions of the protein. Nevertheless, the use of polyclonal antibody against multiple epitopes provides information regarding the extents of the conformational changes in the protein under various functional states.

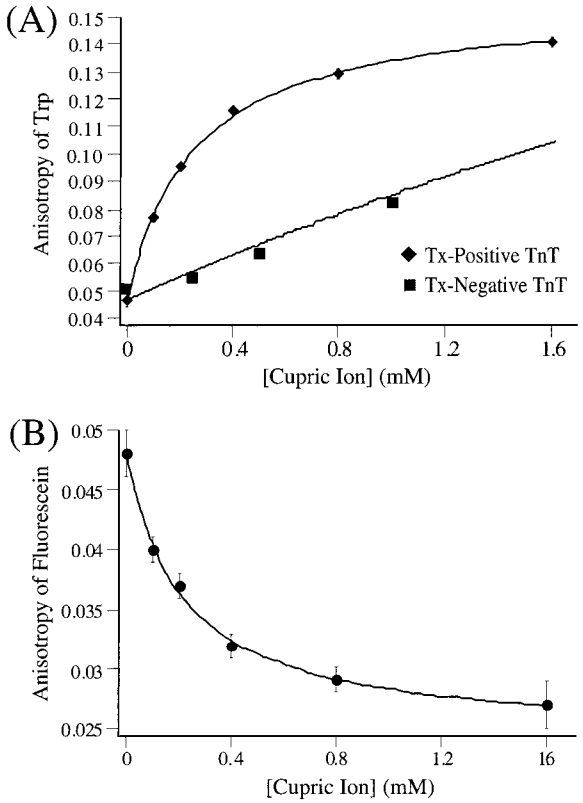

FIGURE 7: Fluorescence anisotropy changes of TnT8e16 in response to Cu(II) binding. (A) Fluorescence anisotropies of intrinsic Trp fluorescence of the Tx-negative and Tx-positive TnT's measured by excitation and emission at 300 and 348 nm, respectively. Significantly different from that of the Tx-negative TnT, the changes induced in the Tx-positive TnT8e16 at 7700 nM are consistent with Cu(II) binding with a dissociation constant of 0.25 ± 0.02 mM, similar to the values obtained from direct fluorescence quenching in Figure 5B. There is a decrease in overall rotational flexibility of the tryptophans upon Cu(II) binding. (B) In contrast, the fluorescence anisotropies in of fluorescein-5 maleimide-labeled Cys_{263} in TnT8-e16 at 120 nM upon the addition of Cu(II), indicating an increase in rotational flexibility of this region of the COOH-terminal portion of TnT8-e16. Similar to the results with Trp fluorescence, the changes in fluorescein-5 maleimide fluorescence are consistent with a dissociation constant of 0.21 ± 0.02 mM for Cu(II) binding. See Experimental Procedures for the nonlinear curve-fitting procedures. The correlation coefficient, r^2, was greater than 0.98 in all cases.

A significantly lower concentration of Cu(II) was required to induce a change in epitope conformation in the antibody-affinity titration against TnT8e16 immobilized onto the microtiter plates (Figure 3A and Table 1) than that for changes detected against free TnT in solution by ELISA (Figure 3B), intrinsic fluorescence of Trp_{234}, Trp_{236}, and Trp_{285} or fluorescein labeling on Cys_{263} (Figures 5, 6B, 7 and Table 2). This significant difference in metal ion-binding affinity between the free TnT8e16 and that immobilized onto the microtiter plates may indicate a higher accessibility or facilitated metal ion binding of the Tx segment in that conformation. Another likely explanation for the difference in apparent affinities between the metal ion binding assays in the liquid and solid phases is the closer association between TnT molecules absorbed to the solid phase. The TnT molecules on the microtiter plate are held in close proximity to each other compared to TnT molecules in solution that are free to diffuse far away from each other or that bound to the immobilized Tm which provides a spatial

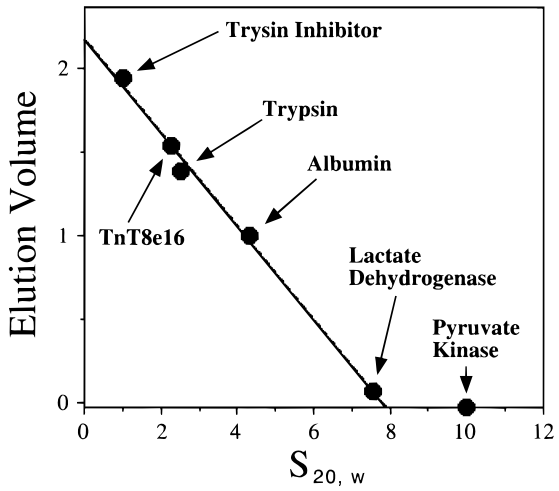

FIGURE 8: Determination of sedimentation coefficient for TnT8e16. Zonal ultracentrifugation was performed in 5−20% sucrose gradients on TnT8e16 and standards of known sedimentation coefficients. The volumes corresponding to the peaks of the major protein bands were recorded and plotted versus the known sedimentation coefficients for the standards. The results determined a $s_{20,w}$ value of 2.3 ± 0.3 for TnT8e16.

framework. It is a well-know phenomenon that if binding sites are held close to each other, their apparent binding affinities are greatly increased; for one of many examples, note the large difference in affinities between many F_{ab} fragments and their parent antibodies. The concentration of metal ions at the surface of the microtiter plate where the TnT is densely packed will be higher than in the rest of the solution, because the metal ions will be bound and released by neighboring TnT molecules. Sometimes microtiter plates can also attract metal ions to their surface. On the other hand, the association of TnT to the Tm framework would eliminate any divalent binding of the anti-TnT antibodies and, therefore, diminish the detection of the conformational changes affecting the high-affinity divalent IgG−TnT interactions. Nevertheless, the mechanisms for the significant difference between the metal-binding affinity of immobilized and free TnT remains to be established.

Biological Significance of the NH_2-Terminus-Modulated Changes in TnT Molecular Conformation and Flexibility. Alternative splicing of the highly variable NH_2-terminal region of TnT is a common developmental process in both cardiac and skeletal muscles (*5*, *13*, *14*). This TnT isoform switch is made by inclusion or exclusion of an acidic segment which alters the charge profile of the NH_2 terminus. The functional role of the alternatively spliced NH_2-terminal variable region of TnT is not fully established but an increased amount of experimental data has shown its importance in the Ca^{2+} regulation of muscle contraction. The demonstration of the effect of the NH_2-terminal physical property of TnT on the global conformation of TnT provides evidence for the biophysical mechanism of the structure−function relationship of TnT and functional significance of the alternatively spliced isoforms. We have previously demonstrated that the binding of metal ions to the NH_2-terminal Tx element of TnT can alter TnT's interactions to Tm, TnI and TnC (*27*, *29*, *42*). The Cu(II)-induced changes in the COOH-terminal conformation of TnT strongly support the NH_2-terminus' role in regulating the structure and function of the COOH-terminal domain that directly binds Tm, TnI and TnC.

The relevance of the findings presented here to the in vivo state depends partly on the extent to which TnT retains its native structure in solution compared to its structure in the myofibril. Upon metal ion binding, the structure of the NH_2 terminus of TnT becomes highly resistant to denaturation by urea as evidenced by the fact that it retains the ability to bind with high affinity and discriminate between different metal ions in the presence or absence of high urea concentrations during affinity chromatography (*28*). This high stability suggests that a significant portion of metal-bound TnT's tertiary structure may be maintained during its incorporation into the thin filament. Since the fluorescein-5 maleimide-labeled Cys_{263} provides a sensitive and specific probe of the TnT conformation, it will be useful in future studies to evaluate the conformational changes of TnT in reconstituted thin filaments and myofibrils. It is worth noting that Cys_{263} is in the COOH-terminal, alternatively spliced region of fast skeletal muscle TnT and may provide a probe to investigate the functional significance of the adult fast skeletal muscle TnT-specific exon 16-encoded segment (*13*, *31*). Although the metal binding Tx−TnT used as a model molecule in this study is only found in two orders of birds (*28*), it is a native TnT with normal function. Therefore, the conformational relationship measured on TnT8e16 has a representative meaning. However, the metal ion-induced change would only occur in this class of TnT isoforms and its biological effect in the avian breast muscle remains to be established. Studies on the TnT fragments showed that NH_2- and COOH-terminal fragments of TnT perform distinct functions (*20*). Our characterizations with different isoforms of TnT or modifications to the structure of the NH_2 terminus are complementary to the analysis using the TnT fragments, which cannot rule out the possibility that communications between the NH_2- and COOH-termini also exist.

An important new finding by the present study is that the NH_2-terminal conformation of TnT also changes the flexibility of the protein structure. This finding provides a new concept to further understand the structure−function relationship of TnT that functions as a signal transduction protein in the allosteric regulatory system of the striated muscle thin filament. Dissection of the conformational and flexibility changes of TnT isoforms may contribute to a better understanding of TnT's role in determining the Ca^{2+} sensitivity (*25*) and cooperativity (*37*) of muscle contraction. The differential responses of the rotational flexibility of Trp_{234}, Trp_{236}, Trp_{285}, and Cys_{263}, all of which are in the COOH-terminal domain of TnT (Figure 1), may indicate an active role of the conformational modification in this functionally important region (Figure 1) in response to the developmentally or pathologically regulated NH_2-terminal structure. It is interesting to note that cardiac TnT mutations deleting the COOH terminus including the Cys_{263} and Trp_{285} region have been found to cause human familial hypertrophic cardiomyopathy (*38*) with alterations in muscle contractility (*39*, *40*). Aberrant splicing of fast skeletal muscle TnT mRNA skipping both exons 16 and 17 can also generate a functional deletion of this region (*31*). Although the COOH-terminus-truncated TnT can incorporate into the myofilaments (*41*), the functional alterations indicate a critical function of this region. Therefore, the modulation of

conformation and flexibility in the COOH-terminal domain of TnT by metal ion binding to the NH_2-terminal variable region supports that the alternatively spliced TnT isoforms varying in the NH_2 terminus constitute an important biological regulation of muscle contraction.

ACKNOWLEDGMENT

We thank Wenhua Chen for technical assistance.

REFERENCES

1. Leavis, P. C., and Gergely, J. (1984) *CRC Crit. Rev. Biochem. 16*, 235−305.
2. Zot, A. S., and Potter, J. D. (1987) *Annu. Rev. Biophys. Biophys. Chem. 16*, 535−559.
3. Tobacman, L. S. (1996) *Annu. Rev. Physiol. 58*, 447−481.
4. Perry, S. V. (1998) *J. Muscle Res. Cell Motil. 19*, 575−602.
5. Cooper, T. A., and Ordahl, C. P. (1985) *J. Biol. Chem. 260*, 11140−11148.
6. Breitbart, R. E., and Nadal-Ginard, B. (1986) *J. Mol. Biol. 188*, 313−324.
7. Jin, J.-P., Huang, Q.-Q., Yeh, H. I., and Lin, J. J.-C. (1992) *J. Mol. Biol. 227*, 1269−1276.
8. Huang, Q.-Q., Chen, A., and Jin, J.-P. (1999) *Gene 229*, 1−10.
9. Bucher, E. A., Dhoot, G. K., Emerson, M. M., Ober, M., and Emerson, C. P., Jr. (1999) *J. Biol. Chem. 274*, 17661−17670.
10. Smillie, L. B., Golosinska, K., and Reinach, F. C. (1988) *J. Biol. Chem. 263*, 18816−18820.
11. Briggs, M. M., and Schachat, F. (1993) *Dev. Biol. 158*, 503−509.
12. Schachat, F., Schmidt, J. M., Maready, M., and Briggs, M. M. (1995) *Dev. Biol. 171*, 233−239.
13. Wang, J., and Jin, J.-P. (1997) *Gene 193*, 105−114.
14. Jin, J.-P., and Lin, J. J.-C. (1988) *J. Biol. Chem. 263*, 7309−7315.
15. Akella, A. B., Ding, X. L., Cheng, R., and Gulati, J. (1995) *Circ. Res. 76*, 600−606.
16. Saba, Z., Nassar, R., Ungerleider, R. M., Oakeley, A. E., and Anderson, P. A. W. (1996) *Circulation 94*, 472−476.
17. Pearlstone, J. R., and Smillie, L. B. (1982) *J. Biol. Chem. 257*, 10587−10592.
18. Heeley, D. H., Golosinska, K., and Smillie, L. B. (1987) *J. Biol. Chem. 262*, 9971−9978.
19. Pearlstone, J. R., and Smillie, L. B. (1985) *Can. J. Biochem. 63*, 212−218.
20. Schaertl, S., Lehrer, S. S., and Geeves, M. A. (1995) *Biochemistry 34*, 15890−15894.
21. Jha, P. K., Leavis, P. C., and Sarkar, S. (1996) *Biochemistry 35*, 16573−16580.
22. Fisher, D., Wang, G., and Tobacman, L. S. (1995) *J. Biol. Chem. 270*, 25455−25460.
23. Pan, B.-S., Gordon, A. M., and Potter, J. D. (1991) *J. Biol. Chem. 266*, 12432−12438.
24. Tobacman, L. S. (1988) *J. Biol. Chem. 263*, 2668−2672.
25. Ogut, O., Granzier, H., and Jin, J.-P. (1999) *Am. J. Physiol.: Cell Physiol. 276*, C1162−1170.
26. Ogut, O., and Jin, J.-P. (1998) *J. Biol. Chem. 273*, 27858−27866.
27. Wang, J., and Jin, J.-P. (1998) *Biochemistry 37*, 14519−14528.
28. Jin, J.-P., and Smillie, L. B. (1994) *FEBS Lett. 341*, 135−140.
29. Ogut, O., and Jin, J.-P. (1996) *Biochemistry 35*, 16581−16590.
30. Arnold, F. H., and Haymore, B. L. (1991) *Science 252*, 1796−1797.
31. Jin, J.-P., Wang, J., and Ogut, O. (1998) *Biochem. Biophys. Res. Commun. 242*, 540−544.
32. Mak, A. S., Golosinska, K., and Smillie, L. B. (1983) *J. Biol. Chem. 258*, 14330−14334.
33. Nozaki, Y. (1990) *Arch. Biochem. Biophys. 277*, 324−333.
34. Cantor, C. R., and Schimmel, P. R. (1980) *Biophysical Chemistry Part II: Techniques for the Study of Biological Structure and Function*, W. H. Freeman and Company, New York.
35. Creighton, T. E. (1993) *Proteins: Structures and Molecular Properties*, W. H. Freeman and Company, New York.
36. Goldberg, M. E. (1991) *TIBS 16*, 358−362.
37. Huang, Q.-Q., Brozovich, F. V., and Jin, J.-P. (1999) *J. Physiol. (London) 520*, 231−242.
38. Watkins, H., McKenna, W. J., Thierfelder, L., Suk, H. J., Anan, R., O'Donoghue, A., Spirito, P., Matsumori, A., Moravec, C. S., Seidman, J. G., and Seidman, C. E. (1995) *N. Engl. J. Med. 332*, 1058−1064.
39. Tobacman, L. S., Lin, D., Butters, C., Landis, C., Back, N., Pavlov, D., and Homsher, E. (1999) *J. Biol. Chem. 274*, 28363−70
40. Mukherjea, P., Tong, L., Seidman, J. G., Seidman, C. E., Hitchcock-DeGregori, S. E. (1999) *Biochemistry 38*, 13296−301.
41. Watkins, H., Seidman, C. E., Seidman, J. G., Feng, H. S., and Sweeney, H. L. (1996) *J. Clin. Invest. 98*, 2456−61.
42. Jin, J.-P.; Chen, A., Ogut, O., and Huang, Q.-Q. (2000) *Am. J. Physiol.: Cell Physiol. 279*, 1067−1077.

BI9927437